

# SAE 4140 (0.015 max S) Steel Iteration #96

## Microstructural Data, Monotonic And Fatigue Test Results

Prepared by:

H. Zhang  
and  
A. Fatemi

Department of Mechanical, Industrial and  
Manufacturing Engineering  
The University of Toledo  
Toledo, Ohio 43606

Prepared for:  
The AISI Bar Steel Applications Group

July 2005



American Iron and Steel Institute  
2000 Town Center, Suite 320  
Southfield, Michigan 48075  
tel: 248-945-4777  
fax: 248-352-1740  
[www.autosteel.org](http://www.autosteel.org)

# TABLE OF CONTENTS

SUMMARY .....	1
<b>I. EXPERIMENTAL PROGRAM .....</b>	<b>2</b>
1.1 MATERIAL AND SPECIMEN FABRICATION .....	2
1.1.1 Material .....	2
1.1.2 Specimen .....	2
1.2 TESTING EQUIPMENT .....	3
1.2.1 Apparatus .....	3
1.2.2 Alignment .....	4
1.3 TEST METHODS AND PROCEDURES .....	4
1.3.1 Monotonic tension tests .....	4
1.3.2 Constant amplitude fatigue tests .....	5
<b>II. EXPERIMENTAL RESULTS AND ANALYSIS.....</b>	<b>7</b>
2.1 MICROSTRUCTURAL DATA .....	7
2.2 MONOTONIC DEFORMATION BEHAVIOR .....	8
2.3 CYCLIC DEFORMATION BEHAVIOR .....	10
2.3.1 Transient cyclic deformation .....	10
2.3.2 Steady-state cyclic deformation .....	10
2.4 CONSTANT AMPLITUDE FATIGUE BEHAVIOR .....	12
<b>REFERENCES.....</b>	<b>30</b>
<b>APPENDIX.....</b>	<b>31</b>

## NOMENCLATURE

$A_o, A_f$	initial, final area	S	engineering stress
HB, HRB, HRC	Brinell, Rockwell B-Scale, Rockwell C-Scale hardness number	YS, UYS, LYS, YS'	monotonic yield, upper yield, lower yield, cyclic yield strength
b, c, n	fatigue strength, fatigue ductility, strain hardening exponent	YPE	yield point elongation
$D_o, D_f$	initial, final diameter	$S_u$	ultimate tensile strength
e	engineering strain	%EL	percent elongation
E, E'	monotonic, midlife cycle modulus of elasticity	%RA	percent reduction in area
K, K'	monotonic, cyclic strength coefficient	$\sigma, \sigma_f, \sigma_f'$	true stress, true fracture strength, fatigue strength coefficient
$L_o, L_f$	initial, final gage length	$\sigma_a, \sigma_m, \Delta\sigma$	stress amplitude, mean stress, stress range
$N_{50\%},$ $(N_f)_{10\%},$ $(N_f)_{50\%},$	number of cycles to midlife, 10% load drop, 50% load drop	$\epsilon_e, \epsilon_p, \epsilon$	true elastic, plastic, total strain
$2N_f$	reversals to failure	$\epsilon_f, \epsilon_f'$	true fracture ductility, fatigue ductility coefficient
$P_f, P_u$	fracture, ultimate load	$\epsilon_a, \epsilon_m, \Delta\epsilon$	strain amplitude, mean strain, strain range
R	neck radius; or strain ratio	$\Delta\epsilon_e, \Delta\epsilon_p$	elastic, plastic strain range

## UNIT CONVERSION TABLE

<u>Measure</u>	<u>SI Unit</u>	<u>US Unit</u>	<u>from SI to US</u>	<u>from US to SI</u>
Length	mm	in	1 mm = 0.03937 in	1 in = 25.4 mm
Area	mm <sup>2</sup>	in <sup>2</sup>	1 mm <sup>2</sup> = 0.00155 in <sup>2</sup>	1 in <sup>2</sup> = 645.16 mm <sup>2</sup>
Load	kN	klb	1kN = 0.2248 klb	1 klb = 4.448 kN
Stress	MPa	ksi	1 MPa = 0.14503 ksi	1 ksi = 6.895 MPa
Temperature	°C	°F	°C = (°F - 32)/1.8	°F = (°C * 1.8) + 32

<u>In SI Unit:</u>	1 kN = 10 <sup>3</sup> N	1 Pa = 1 N/m <sup>2</sup>	1 MPa = 10 <sup>6</sup> Pa = 1 N/mm <sup>2</sup>	1 Gpa = 10 <sup>9</sup> Pa
<u>In US Unit:</u>	1 klb = 10 <sup>3</sup> lb	1 psi = 1 lb/in <sup>2</sup>	1 ksi = 10 <sup>3</sup> psi	

## **SUMMARY**

The microstructural data, monotonic properties, and fatigue behavior data have been obtained for SAE 4140 steel with max. 0.015 S. The material was provided by the American Iron and Steel Institute (AISI). Microstructural data includes grain type, grain size, and inclusion content. Two tensile tests were performed to acquire the desired monotonic properties. Eighteen strain-controlled fatigue tests were performed to obtain the strain-life and cyclic stress-strain curves and properties. The experimental procedure followed and results obtained are presented and discussed in this report.

# I. EXPERIMENTAL PROGRAM

## 1.1 Material and Specimen Fabrication

### 1.1.1 Material

The SAE 4140 (0.015 max S) steel was manufactured and induction hardened by MacSteel Company. This material was delivered to the University of Toledo in circular bar form. The bars were approximately 1.12 inch in diameter prior to machining. In Table 1, the chemical composition supplied by MacSteel Company is shown.

### 1.1.2 Specimen

In this study, identical round specimens were used for the monotonic and fatigue tests. The specimen configuration and dimensions are shown in Figure 1. This configuration deviates slightly from the specimens recommended by ASTM Standard E606 [1]. The recommended specimens have uniform or hourglass test sections. The specimen geometry shown in Figure 1 differs by using a large secondary radius throughout the test section.

All specimens were machined in the Mechanical, Industrial, and Manufacturing Engineering Machine Shop at the University of Toledo. The bars from which the specimens were made were induction hardened at the mill. Using the CNC machine, the tolerable dimensions specified on the specimen drawings final turning was achieved. Then the specimens were polished.

A commercial round-specimen polishing machine was used to polish the specimen gage section. Four different grits of aluminum oxide lapping film were used: 30 $\mu$ , 15 $\mu$ , 9 $\mu$ , and 3 $\mu$ . The 3 $\mu$  grit was used as the final polish and polishing marks coincided with the specimens' longitudinal direction. The polished surfaces were carefully examined under magnification to ensure complete removal of machine marks within the test section.

## **1.2 Testing Equipment**

### **1.2.1 Apparatus**

An INSTRON 8801 closed-loop servo-hydraulic axial load frame in conjunction with a Fast-Track digital servo-controller was used to conduct the tests. The calibration of this system was verified prior to beginning the test program. The load cell used had a capacity of 11 klb. Hydraulically operated grips using universal tapered collets were employed to secure the specimens' ends in series with the load cell.

Total strain was controlled for all tests using an extensometer rated as ASTM class B1 [2]. The calibration of the extensometer was verified using displacement apparatus containing a micrometer barrel in divisions of 0.0001 in. The extensometer had a gage length of 0.30 in and was capable of measuring strains up to 15 %.

In order to protect the specimens' surface from the knife-edges of the extensometer, ASTM Standard E606 recommends the use of transparent tape or epoxy to 'cushion' the attachment. For this study, it was found that application of transparent tape strips was difficult due to the radius within the test section. Therefore, epoxy was

considered to be the best protection. One disadvantage of epoxy is the variability of mixtures throughout the test program. As an alternative to epoxy, M-coat D offered a more consistent mixture. Therefore, the tests were performed using M-coat D.

### **1.2.2 Alignment**

Significant effort was put forth to align the load train (load cell, grips, specimen, and actuator). Misalignment can result from both tilt and offset between the central lines of the load train components. According to ASTM Standard E606, the maximum bending strains should not exceed 5 % of the minimum axial strain range imposed during any test program. For this study, the minimum axial strain range was 0.006 in/in. Therefore, the maximum allowable bending strain was 300 microstrain. ASTM Standard E1012, Type A, Method 1 was followed to verify specimen alignment [3]. For this procedure, two arrays of four strain gages per array were arranged at the upper and lower ends of the uniform gage section. For each array, gages were equally spaced around the circumference of a 0.5-in. uniform diameter bar. The maximum bending strain determined from the gauged specimen was less than 60 microstrain. This value was well within the allowable ASTM limit.

## **1.3 Test Methods and Procedures**

### **1.3.1 Monotonic tension tests**

All monotonic tests in this study were performed using test methods specified by ASTM Standard E8 [4]. Three specimens were used to obtain the monotonic properties.



Due to the limitations of the extensometer, strain control was used only up to 14% strain. After this point, displacement control was used until fracture.

For the elastic and initial yield region (0% to 0.5% strain), a strain rate of 0.0025 in/in/min was chosen. This strain rate was three-quarters of the maximum allowable rate specified by ASTM Standard E8 for the initial yield region. After yielding (0.5% to 14% strain), the strain rate was increased by a factor of three (i.e., 0.0075 in/in/min). After the extensometer was removed, a displacement rate of 0.01275 in/min was used. This displacement rate provided approximately the same strain rate as that used prior to switching control modes.

After the tension tests were concluded, the broken specimens were carefully reassembled. The final gage lengths of the fractured specimens were measured with a Vernier caliper having divisions of 0.001 in. Using an optical comparator with 10X magnification and divisions of 0.001 in, the final diameter and the neck radius were measured. It should be noted that prior to the test, the initial minimum diameter was measured with this same instrument.

### **1.3.2 Constant amplitude fatigue tests**

All constant amplitude fatigue tests in this study were performed according to ASTM Standard E606. It is recommended by this standard that at least 10 specimens be used to generate the fatigue properties. For this study, 18 specimens at 6 different strain amplitudes ranging from 0.3% to 2% were utilized. INSTRON LCF software was used in all the strain-controlled tests. During each strain-controlled test, the total strain was

recorded using the extensometer output. Test data were automatically recorded throughout each test.

There were two control modes used for these tests. Strain control was used in all tests with plastic deformation. For some of the elastic tests, strain control was used initially to determine the stabilized load, then load control was used for the remainder of the test, and for the rest of the elastic tests, load control was used throughout. The reason for the change in control mode was due to limitations on the extensometer for high test frequencies. For the strain control tests, the applied frequencies ranged from 0.2 Hz to 2 Hz in order to keep a strain rate about 0.02 in/in/sec. For the load control tests, the frequency was increased to 18 Hz in order to shorten the overall test duration. All tests were conducted using a triangular waveform.

## II. EXPERIMENTAL RESULTS AND ANALYSIS

### 2.1 Microstructure Data

Photomicrographs of the microstructure were obtained using an optical microscope with a digital camera attachment. It was observed that the grains in the transverse and longitudinal directions had negligible difference. In Figure 2a and 2b, the microstructure pictures in the longitudinal (L-T) direction and the transverse (T'-T) direction are shown at 500X magnification, respectively. It can be seen from these photomicrographs that SAE 4140 (0.015 max S) steel had a martensite microstructure. In Figure 3a and 3b, the inclusions in L-T and T'-T directions are shown at 100X magnification. For Figures 2a and 3a, the rolling direction is parallel to the page, and for Figures 2b and 3b, the rolling direction is perpendicular to the page.

The average grain size was measured in both transverse and longitudinal directions using the comparison procedure reported in ASTM Standard E112 [5]. According to ASTM Standard E45, method A, the inclusion rating numbers for type D inclusion in both L-T and L-T' directions were found [6]. Brinell and Rockwell hardness tests were also performed. A summary of the microstructure data for SAE 4140 (0.015 max S) steel is provided in Table 2.

## 2.2 Monotonic Deformation Behavior

The properties determined from monotonic tests were the following: modulus of elasticity (E), yield strength (YS), ultimate tensile strength ( $S_u$ ), percent elongation (%EL), percent reduction in area (%RA), true fracture strength ( $\sigma_f$ ), true fracture ductility ( $\epsilon_f$ ), strength coefficient (K), and strain hardening exponent (n).

True stress ( $\sigma$ ), true strain ( $\epsilon$ ), and true plastic strain ( $\epsilon_p$ ) were calculated from engineering stress (S) and engineering strain (e), according to the following relationships which are based on constant volume assumption:

$$\sigma = S(1 + e) \quad (1a)$$

$$\epsilon = \ln(1 + e) \quad (1b)$$

$$\epsilon_p = \epsilon - \epsilon_e = \epsilon - \frac{\sigma}{E} \quad (1c)$$

The true stress ( $\sigma$ ) - true strain ( $\epsilon$ ) plot is often represented by the Ramberg-Osgood equation:

$$\epsilon = \epsilon_e + \epsilon_p = \frac{\sigma}{E} + \left( \frac{\sigma}{K} \right)^{\frac{1}{n}} \quad (2)$$

The strength coefficient, K, and strain hardening exponent, n, are the intercept and slope of the best line fit to true stress ( $\sigma$ ) versus true plastic strain ( $\epsilon_p$ ) data in log-log scale:

$$\sigma = K \left( \epsilon_p \right)^n \quad (3)$$

In accordance with ASTM Standard E739 [7], when performing the least squares fit, the true plastic strain ( $\epsilon_p$ ) was the independent variable and the stress ( $\sigma$ ) was the

dependent variable. These plots for the three tests conducted are shown in Figure 4. To generate the K and n values, the range of data used in this figure was chosen according to the definition of discontinuous yielding specified in ASTM Standard E646 [8]. Therefore, the valid data range occurred between the end of yield point extension and the strain at or prior to maximum load.

The true fracture strength,  $\sigma_f$ , was corrected for necking according to the Bridgman correction factor [10]:

$$\sigma_f = \frac{\frac{P_f}{A_f}}{\left(1 + \frac{4R}{D_f}\right) \ln\left(1 + \frac{D_f}{4R}\right)} \quad (4)$$

where  $P_f$  is the load at fracture, R is the neck radius, and  $D_f$  is the diameter at fracture.

The true fracture ductility,  $\epsilon_f$ , was calculated from the relationship based on constant volume:

$$\epsilon_f = \ln\left(\frac{A_o}{A_f}\right) = \ln\left(\frac{1}{1 - RA}\right) \quad (5)$$

where  $A_f$  is the cross-sectional area at fracture,  $A_o$  is the original cross-sectional area, and RA is the reduction in area.

A summary of the monotonic properties for SAE 4140 (0.015 max S) steel is provided in Table 2. The monotonic stress-strain curves are shown in Figure 5. As can be seen from this figure, the two curves are very close to each other. Refer to Table A.1 in the Appendix for a summary of the monotonic test results.

## **2.3 Cyclic Deformation Behavior**

### **2.3.1 Transient cyclic response**

Transient cyclic response describes the process of cyclic-induced change in deformation resistance of a material. Data obtained from constant amplitude strain-controlled fatigue tests were used to determine this response. Plots of stress amplitude variation versus applied number of cycles can indicate the degree of transient cyclic softening/hardening. Also, these plots show when cyclic stabilization occurs. A composite plot of the transient cyclic response for SAE 4140 (0.015 max S) steel is shown in Figure A.1 of the Appendix. The transient response was normalized on the rectangular plot in Figure A.1a, while a semi-log plot is shown in Figure A.1b. Even though multiple tests were conducted at each strain amplitude, data from one test at each strain amplitude tested are shown in these plots.

### **2.3.2 Steady-state cyclic deformation**

Another cyclic behavior of interest was the steady state or stable response. Data obtained from constant amplitude strain-controlled fatigue tests were also used to determine this response. The properties determined from the steady-state hysteresis loops were the following: cyclic modulus of elasticity ( $E'$ ), cyclic strength coefficient ( $K'$ ), cyclic strain hardening exponent ( $n'$ ), and cyclic yield strength ( $YS'$ ). Half-life (midlife) hysteresis loops and data were used to obtain the stable cyclic properties.

Similar to monotonic behavior, the cyclic true stress-strain behavior can be characterized by the Ramberg-Osgood type equation:

$$\frac{\Delta \varepsilon}{2} = \frac{\Delta \varepsilon_e}{2} + \frac{\Delta \varepsilon_p}{2} = \frac{\Delta \sigma}{2 E} + \left( \frac{\Delta \sigma}{2 K'} \right)^{\frac{1}{n'}} \quad (6)$$

It should be noted that in Equation 7 and the other equations that follow, E is the average modulus of elasticity that was calculated from the monotonic tests.

The cyclic strength coefficient, K', and cyclic strain hardening exponent, n', are the intercept and slope of the best line fit to true stress amplitude ( $\Delta\sigma/2$ ) versus true plastic strain amplitude ( $\Delta\varepsilon_p/2$ ) data in log-log scale:

$$\frac{\Delta \sigma}{2} = K' \left( \frac{\Delta \varepsilon_p}{2} \right)^{n'} \quad (7)$$

In accordance with ASTM Standard E739, when performing the least squares fit, the true plastic strain amplitude ( $\Delta\varepsilon_p/2$ ) was the independent variable and the stress amplitude ( $\Delta\sigma/2$ ) was the dependent variable. The true plastic strain amplitude was calculated by the following equation:

$$\frac{\Delta \varepsilon_p}{2} = \frac{\Delta \varepsilon}{2} - \frac{\Delta \sigma}{2 E} \quad (8)$$

This plot is shown in Figure 6. To generate the K' and n' values, the range of data used in the figure was chosen for  $[\Delta\varepsilon_p/2]_{\text{calculated}} \geq 0.0010$  in/in.

The cyclic stress - strain curve reflects the resistance of a material to cyclic deformation and can be vastly different from the monotonic stress - strain curve. The cyclic stress - strain curve is shown in Figure 7. In Figure 8, superimposed plots of monotonic and cyclic curves are shown. As can be seen in Figure 8, SAE 4140 (0.015 max S) steel cyclically softens. Figure A.2 in the Appendix shows a composite plot of the steady-state (midlife) hysteresis loops. Even though multiple tests were conducted at each

strain amplitude, the stable loops from only one test at each strain amplitude are shown in this plot.

## 2.4 Constant Amplitude Fatigue Behavior

Constant amplitude strain-controlled fatigue tests were performed to determine the strain-life curve. The following equation relates the true strain amplitude to the fatigue life:

$$\frac{\Delta \varepsilon}{2} = \frac{\Delta \varepsilon_e}{2} + \frac{\Delta \varepsilon_p}{2} = \frac{\sigma'_f}{E} (2 N_f)^b + \varepsilon'_f (2 N_f)^c \quad (9)$$

where  $\sigma'_f$  is the fatigue strength coefficient,  $b$  is the fatigue strength exponent,  $\varepsilon'_f$  is the fatigue ductility coefficient,  $c$  is the fatigue ductility exponent,  $E$  is the monotonic modulus of elasticity, and  $2N_f$  is the number of reversals to failure (which was defined as a 50% load drop, as recommended by ASTM Standard E606).

The fatigue strength coefficient,  $\sigma'_f$ , and fatigue strength exponent,  $b$ , are the intercept and slope of the best line fit to true stress amplitude ( $\Delta\sigma/2$ ) versus reversals to failure ( $2N_f$ ) data in log-log scale:

$$\frac{\Delta \sigma}{2} = \sigma'_f (2 N_f)^b \quad (10)$$

In accordance with ASTM Standard E739, when performing the least squares fit, the stress amplitude ( $\Delta\sigma/2$ ) was the independent variable and the reversals to failure ( $2N_f$ ) was the dependent variable. This plot is shown in Figure 9. To generate the  $\sigma'_f$  and  $b$  values, the range of data used in this figure was chosen for  $N_f \leq 10^6$  cycles.



The fatigue ductility coefficient,  $\varepsilon_f'$ , and fatigue ductility exponent,  $c$ , are the intercept and slope of the best line fit to calculated true plastic strain amplitude ( $\Delta\varepsilon_p/2$ ) versus reversals to failure ( $2N_f$ ) data in log-log scale:

$$\left( \frac{\Delta\varepsilon_p}{2} \right)_{\text{calculated}} = \varepsilon_f' (2N_f)^c \quad (11)$$

In accordance with ASTM Standard E739, when performing the least squares fit, the calculated true plastic strain amplitude ( $\Delta\varepsilon_p/2$ ) was the independent variable and the reversals to failure ( $2N_f$ ) was the dependent variable. The calculated true plastic strain amplitude was determined from Equation 8. This plot is shown in Figure 10. To generate the  $\varepsilon_f'$  and  $c$  values, the range of data used in this figure was chosen for  $[\Delta\varepsilon_p/2]_{\text{calculated}} \geq 0.0010$  in/in.

The true strain amplitude versus reversals to failure plot is shown in Figure 11. This plot displays the strain - life curve (Eqn. 9), the elastic strain portion (Eqn. 10), the plastic strain portion (Eqn. 11), and superimposed fatigue data.

A parameter often used to characterize fatigue behavior at stress concentrations, such as at the root of a notch, is Neuber's parameter [10]. Neuber's stress range is given by:

$$\sqrt{(\Delta\varepsilon)(\Delta\sigma)E} = 2\sqrt{(\sigma_f')^2 (2N_f)^{2b} + \sigma_f' \varepsilon_f' E (2N_f)^{b+c}} \quad (12)$$

Plot of Neuber stress range versus reversals to failure is shown in Figure 12. This figure displays the Neuber curve based on Eqn. 12 and superimposed fatigue data for this material.

A comparison of true strain versus reversals to failure between this material and SAE 4140 (0.077S) steel is shown in Figure 13. It can be seen that these two materials have nearly identical fatigue behavior.

A summary of the cyclic properties for SAE 4140 (0.015 max S) steel is provided in Table 2. Table A.2 in the Appendix provides the summary of the fatigue test results.

Table 1: Chemical composition of SAE 4140 (0.015 max S) steel

<b><u>Element</u></b>	<b><u>Wt. %</u></b>
Carbon, C	0.408%
Manganese, Mn	0.920%
Phosphorus, P	0.013%
Sulfur, S	0.015%
Silicon, Si	0.28%
Vanadium, V	0.006%
Chromium, Cr	1%
Aluminum, Al	0.037%
Nickel, Ni	0.15%
Molybdenum, Mo	0.22%
Copper, Cu	0.200%

**Table 2: Summary of the Mechanical Properties**

<b>Microstructural Data</b>	<b>Average</b>			
<b>ASTM grain size number (MAG=500X):</b>				
Transverse direction (T-T')	5 to 6			
Longitudinal direction (L-T)	5 to 6			
<b>Inclusion rating number (MAG=100X):</b>				
Type A (sulfide type), thin series	L-T: 1.5, thin			
Type B (alumina type), thin series	none			
Type C (silicate type), thin series	none			
Type D (globular type), thin series	L-T: 1.5, thin; T-T': 1.5, thin			
<b>Hardness:</b>				
<b>Brinell (HB)</b>				
Transverse direction (T-T')	409.3			
Longitudinal direction (L-T)	NA			
<b>Rockwell B-scale (HRB)</b>				
Transverse direction (T-T')	113.0			
Longitudinal direction (L-T)	NA			
<b>Rockwell C-scale (HRC)</b>				
Transverse direction (T-T')	41.7			
Longitudinal direction (L-T)	NA			
<b>Microstructure type:</b>				
Transverse direction (T-T')	martensite			
Longitudinal direction (L-T)	martensite			
<b>Monotonic Properties</b>	<b>Average</b>		<b>Range</b>	
Modulus of elasticity, E, GPa (ksi):	202.5	(29,368.6)	201.2 - 203.7	(29,186.8 - 29,550.4)
Yield strength (0.2% offset), YS, MPa (ksi):	1157.5	(167.9)	1150.0 - 1165.1	(166.8 - 169.0)
Upper yield strength UYS, MPa (ksi):	NA	NA		
Lower yield strength LYS, MPa (ksi):	NA	NA		
Yield point elongation, YPE (%):	NA			
Ultimate strength, S <sub>u</sub> , MPa (ksi):	1247.8	(181.0)	1243.3 - 1252.4	(180.3 - 181.6)
Percent elongation, %EL (%):	24.50%		24.00% - 25.00%	
Percent reduction in area, %RA (%):	47.5%		45.9% - 49.2%	
Strength coefficient, K, MPa (ksi):	1,498.5	(217.3)	1,498.3 - 1,498.6	(217.3 - 217.3)
Strain hardening exponent, n:	0.0440		0.0429 - 0.0450	
True fracture strength, σ <sub>f</sub> *, MPa (ksi):	1311.3	(190.2)	1311.3 - 1311.3	(190.2 - 190.2)
True fracture ductility, ε <sub>f</sub> (%):	64.55%		61.40% - 67.70%	
<b>Cyclic Properties</b>	<b>Average</b>		<b>Range</b>	
Cyclic modulus of elasticity, E', GPa (ksi):	195.4	(28,340.1)	183.2 - 212.4	(26,563.5 - 30,802.0)
Fatigue strength coefficient, σ <sub>f</sub> <sup>'</sup> , MPa (ksi):	1,601.1	(232.2)		
Fatigue strength exponent, b:	-0.0674			
Fatigue ductility coefficient, ε <sub>f</sub> <sup>'</sup> :	1.2665			
Fatigue ductility exponent, c:	-0.7207			
Cyclic yield strength, YS', MPa (ksi)	855.8	(124.1)		
Cyclic strength coefficient, K', MPa (ksi):	1,695.9	(246.0)		
Cyclic strain hardening exponent, n':	0.1101			
Fatigue strength @ 10 <sup>6</sup> cycles, S <sub>6</sub> , MPa (ksi):	601.9	(87.3)		

\* The values of true fracture strength are corrected for necking according to the Bridgman correction factor.

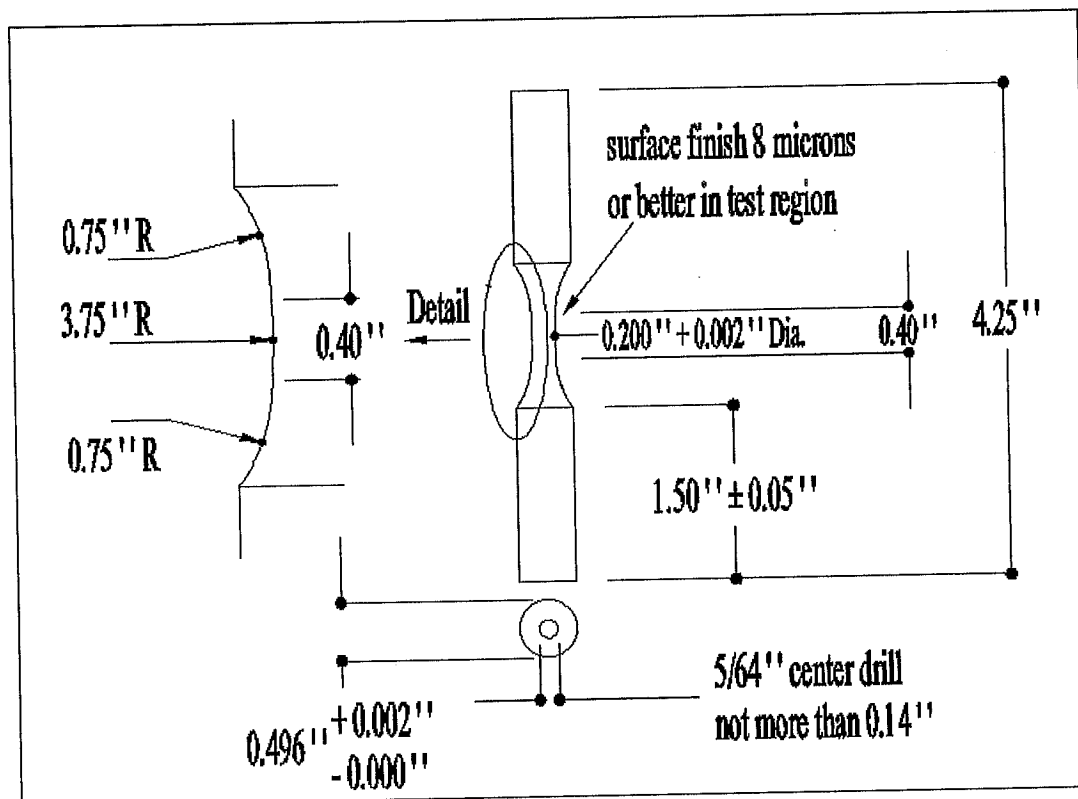


Figure 1: Specimen configuration and dimensions

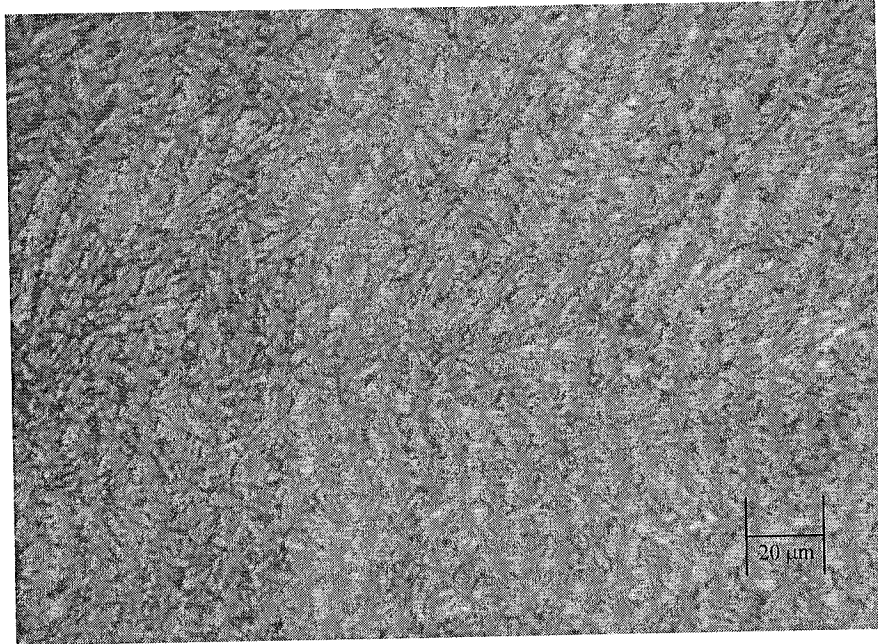


Figure 2a: Photomicrograph in the longitudinal direction (L-T) at 500X for SAE 4140 (0.015 max S) steel (rolling direction is parallel to the page).

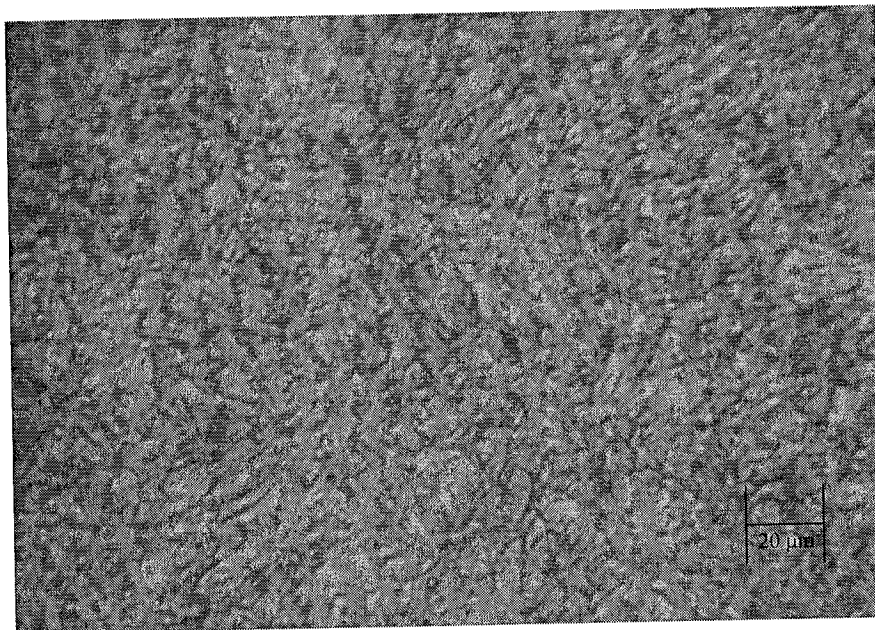


Figure 2b: Photomicrograph in the transverse direction (T-T) at 500X for SAE 4140 (0.015 max S) steel (rolling direction is perpendicular to the page).

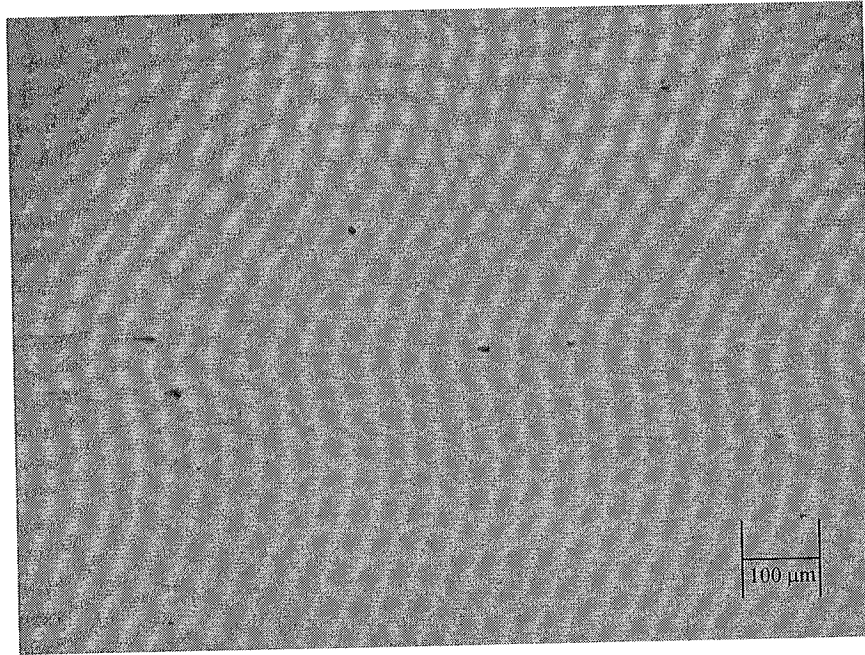


Figure 3a: Examples of inclusions in the longitudinal direction (L-T) at 100X for SAE 4140 (0.015 max S) steel (rolling direction is parallel to the page).

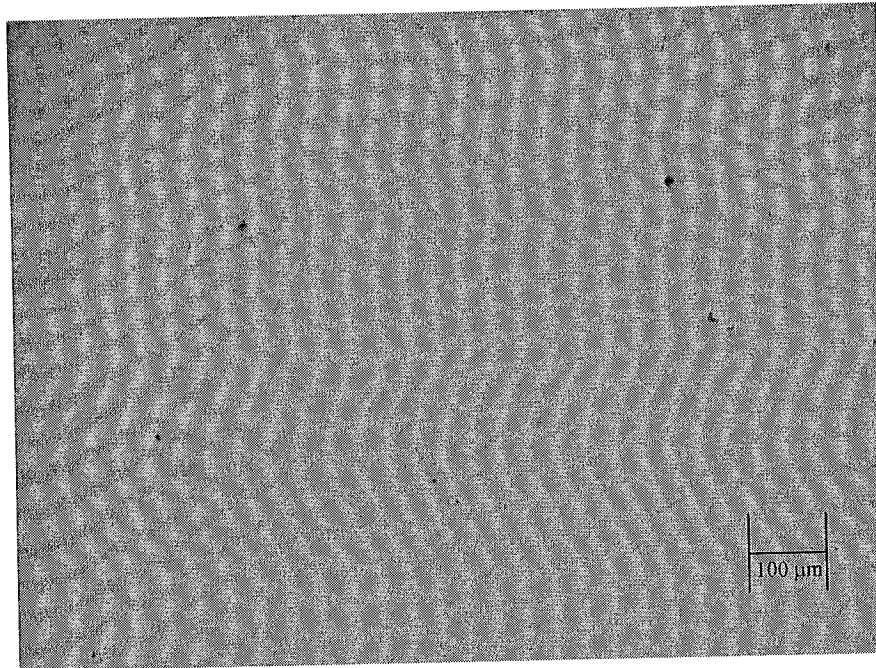


Figure 3b: Examples of inclusions in the second longitudinal direction (L-T') at 100X for SAE 4140 (0.015 max S) steel (rolling direction is perpendicular to the page).

**True Stress vs. True Plastic Strain**

G4-19:  
 $\sigma = 1498.6(\epsilon_p)^{0.0429}$   
 K = 1498.6MPa  
 n = 0.0429  
 $R^2 = 0.9766$

G4-23:  
 $\sigma = 1498.3(\epsilon_p)^{0.045}$   
 K = 1498.3MPa  
 n = 0.045  
 $R^2 = 0.9773$

Specimen ID:  
 (top to bottom)  
 G4-19  
 G4-23

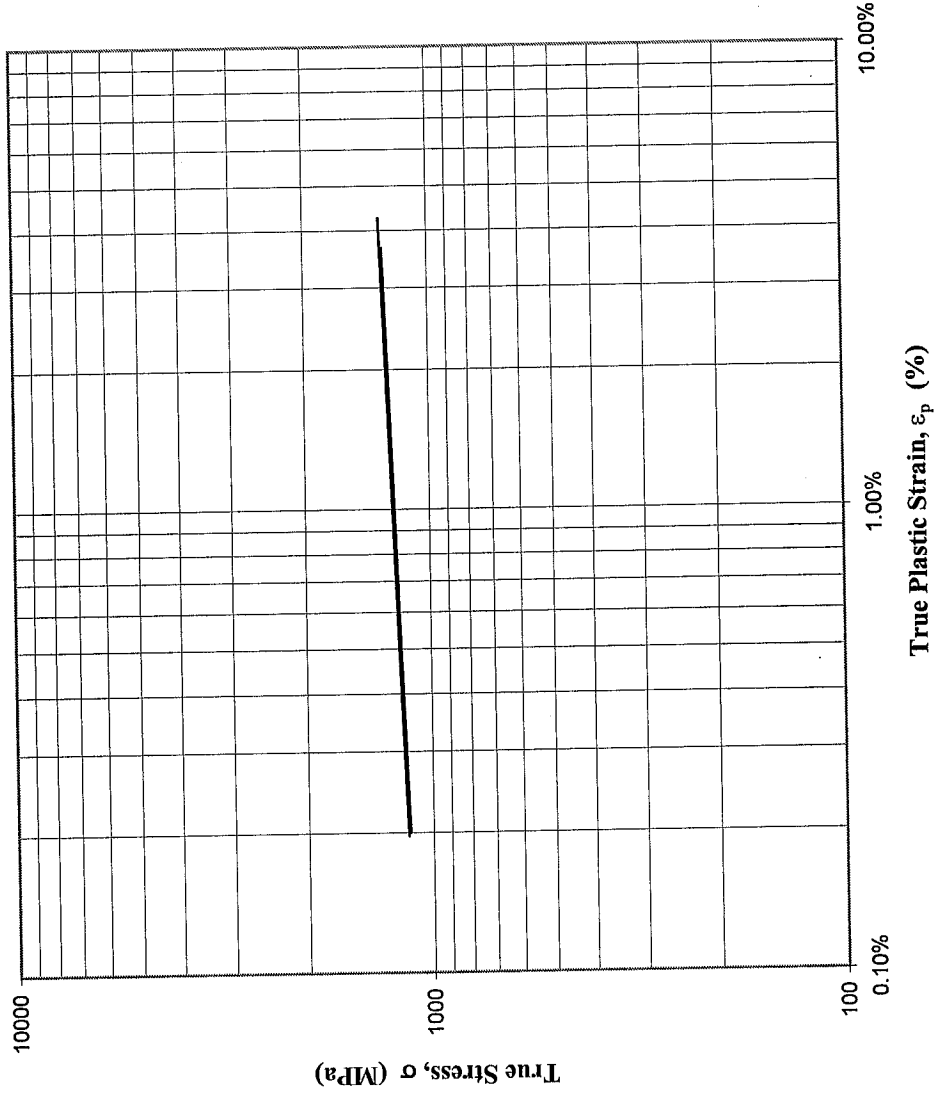


Figure 4: True stress versus true plastic strain



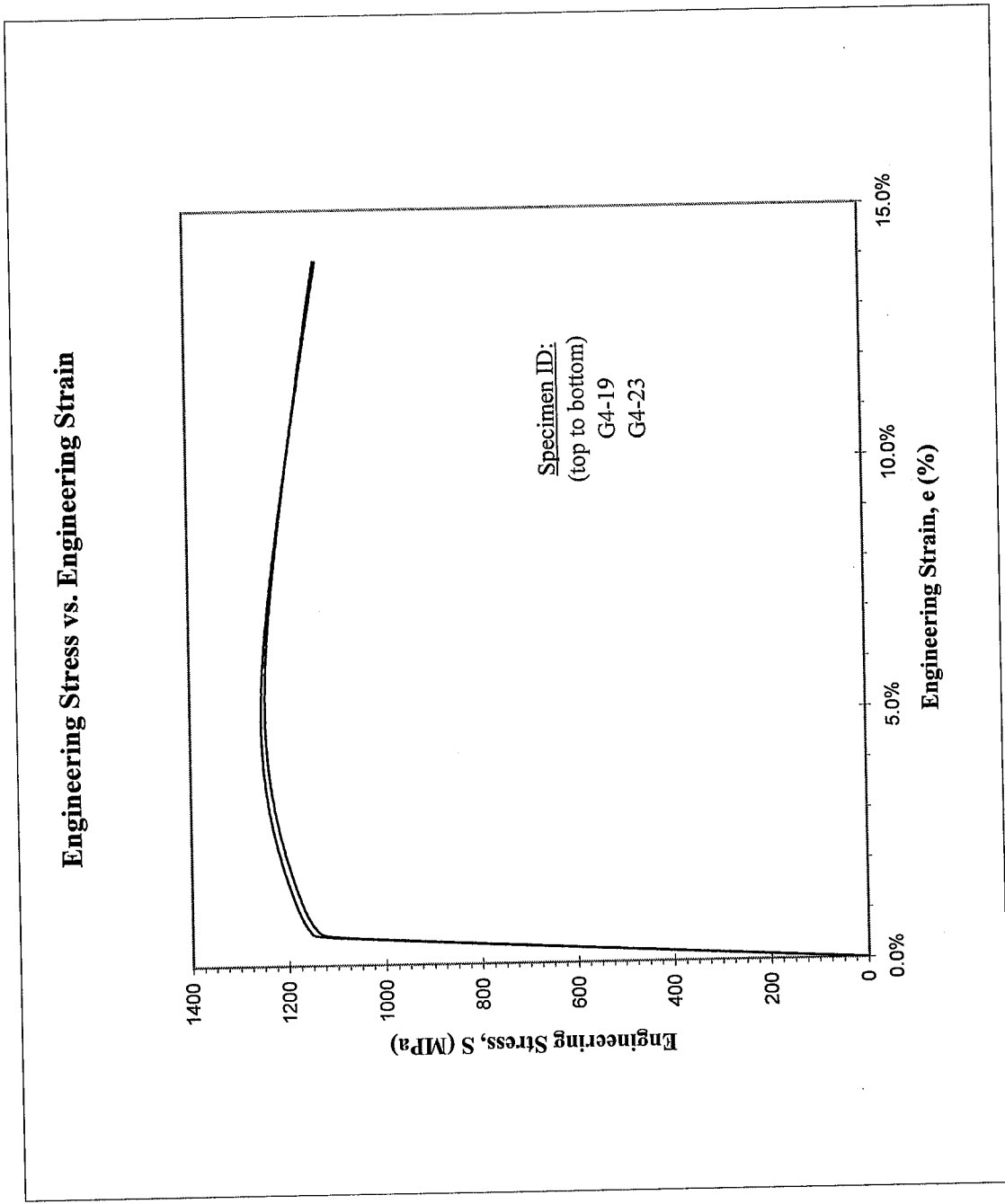


Figure 5: Monotonic stress-strain curve

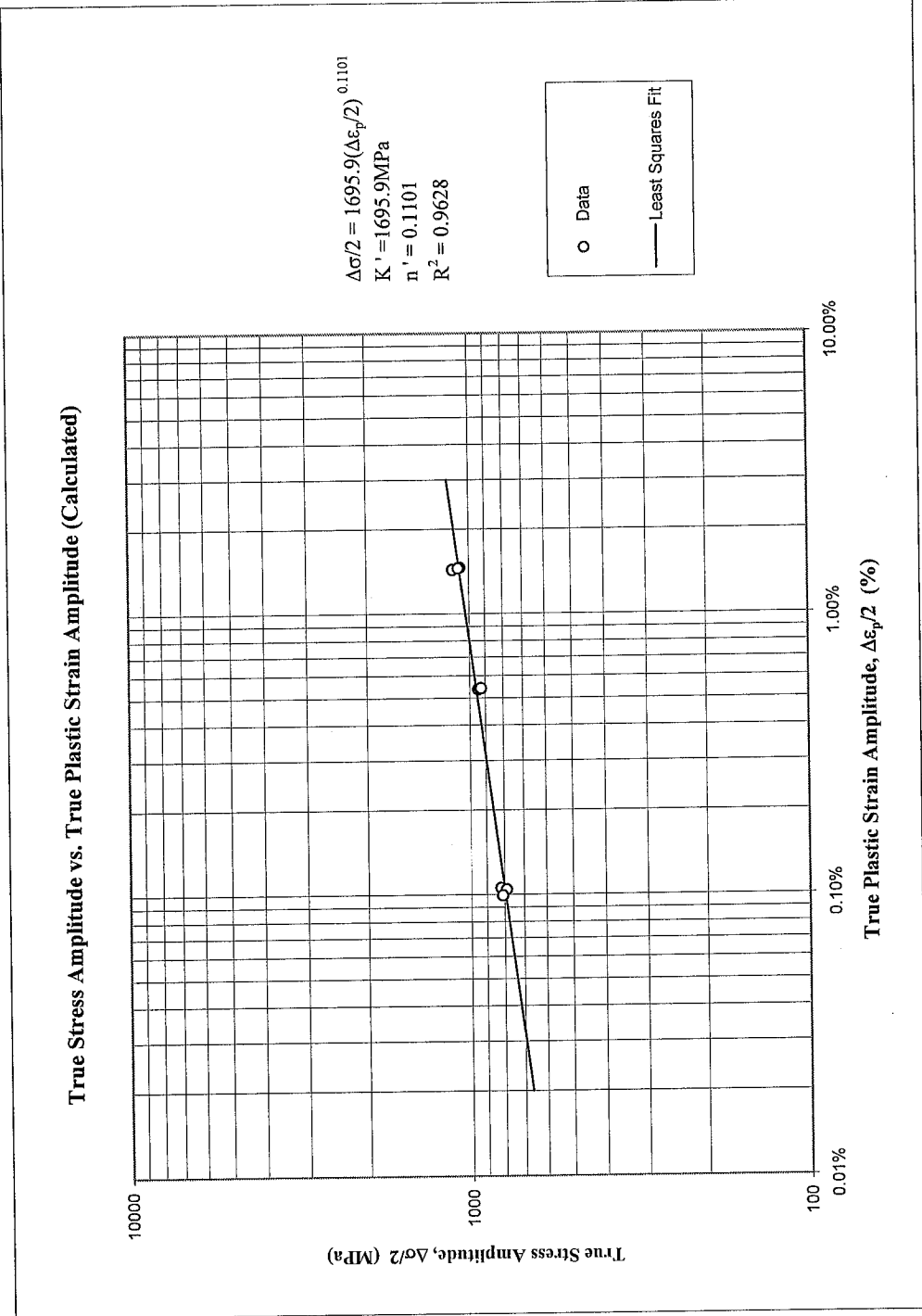


Figure 6: True stress amplitude versus calculated true plastic strain amplitude

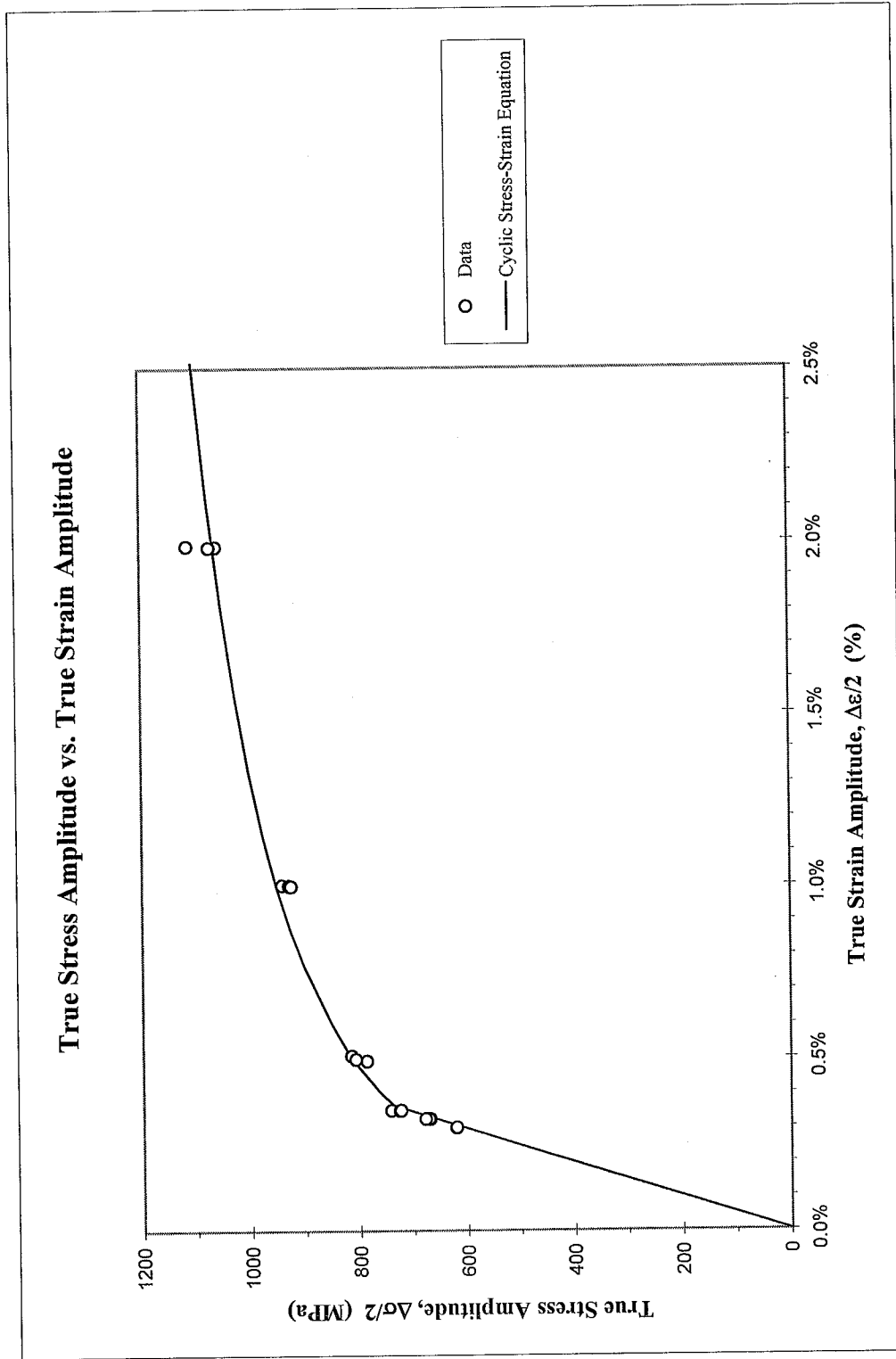


Figure 7: True stress amplitude versus true strain amplitude

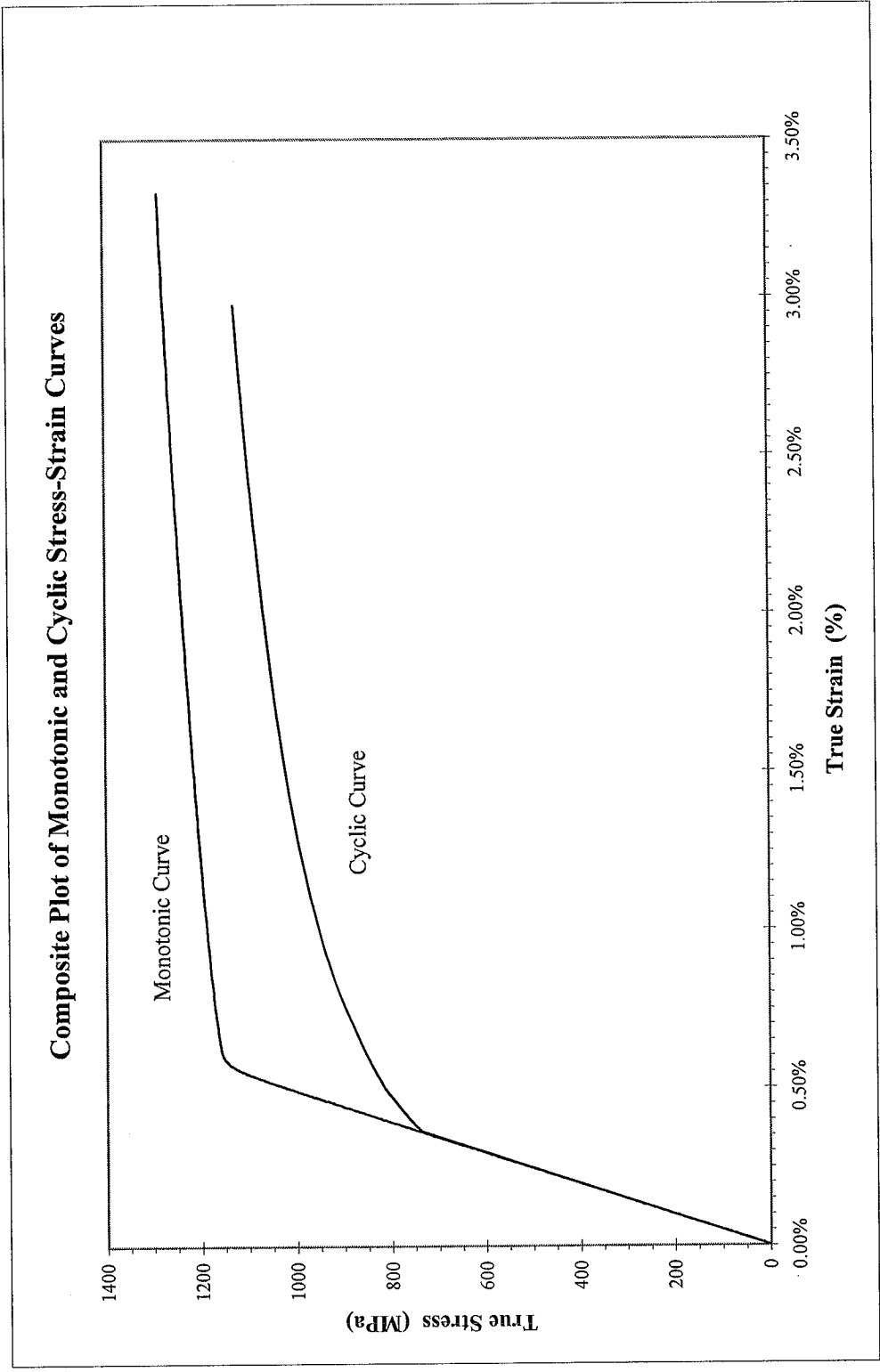


Figure 8: Composite plot of cFcllc and monotonic stress-strain curves

### True Stress Amplitude vs. Reversals to Failure

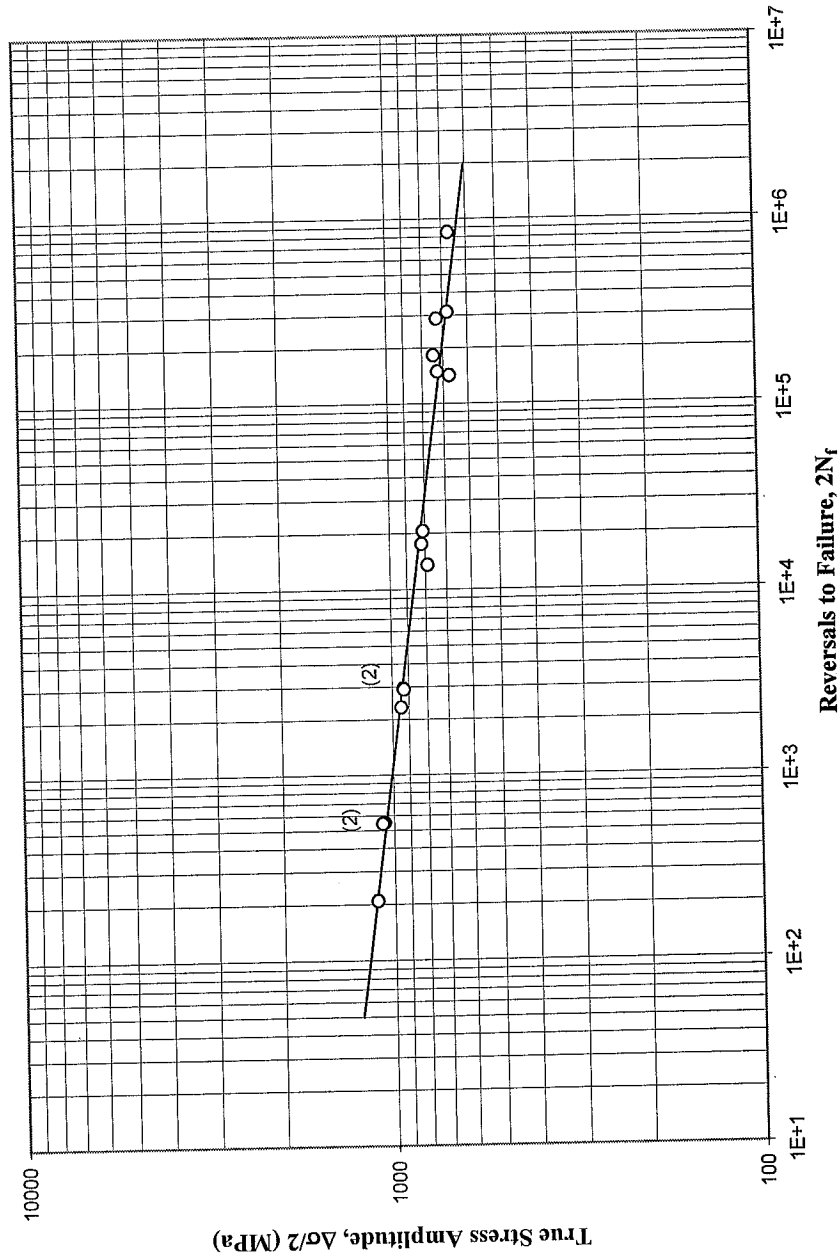


Figure 9: True stress amplitude versus reversals to failure

True Plastic Strain Amplitude (Calculated) vs. Reversals to Failure

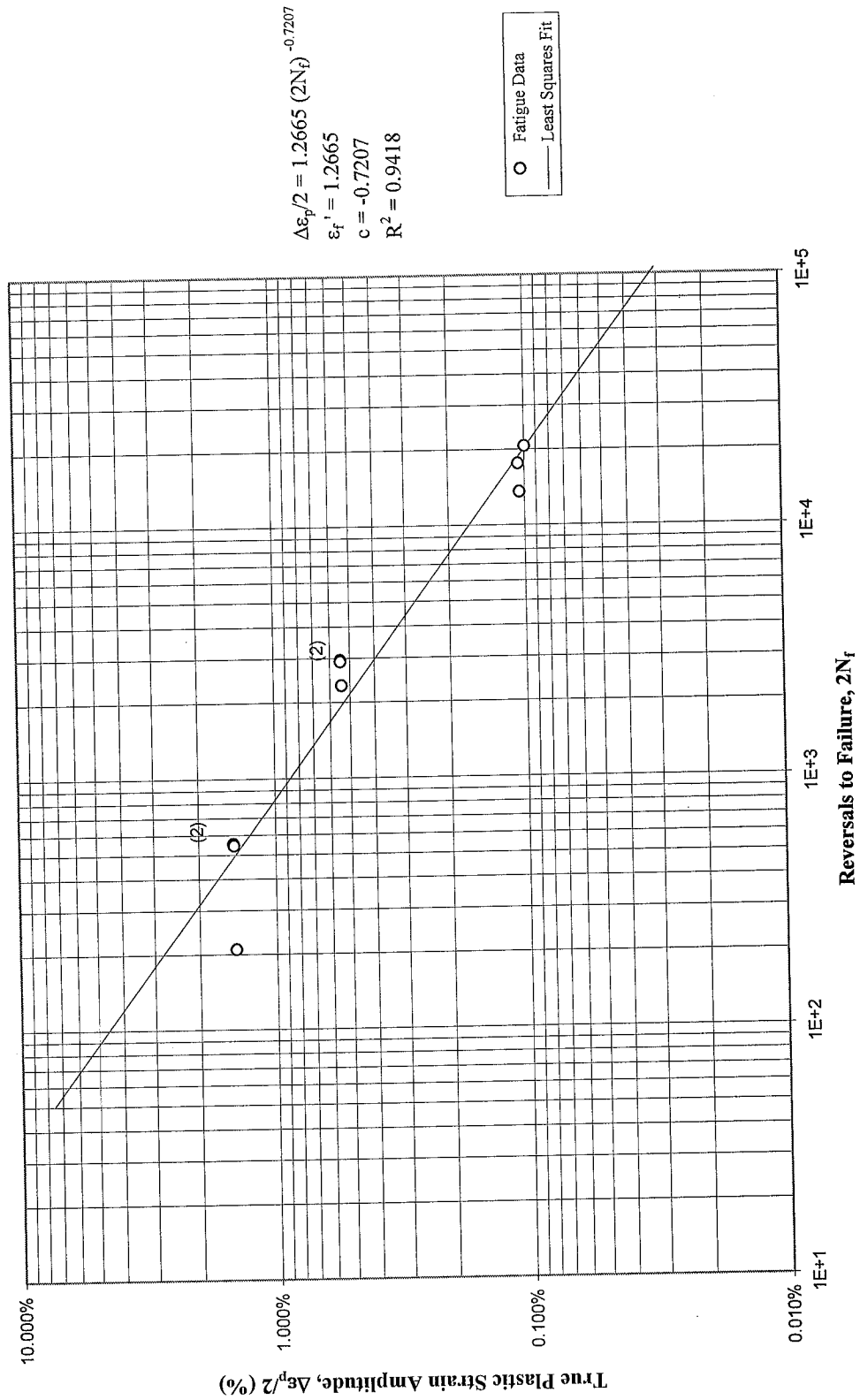


Figure 10: Calculated true plastic strain amplitude versus reversals to failure

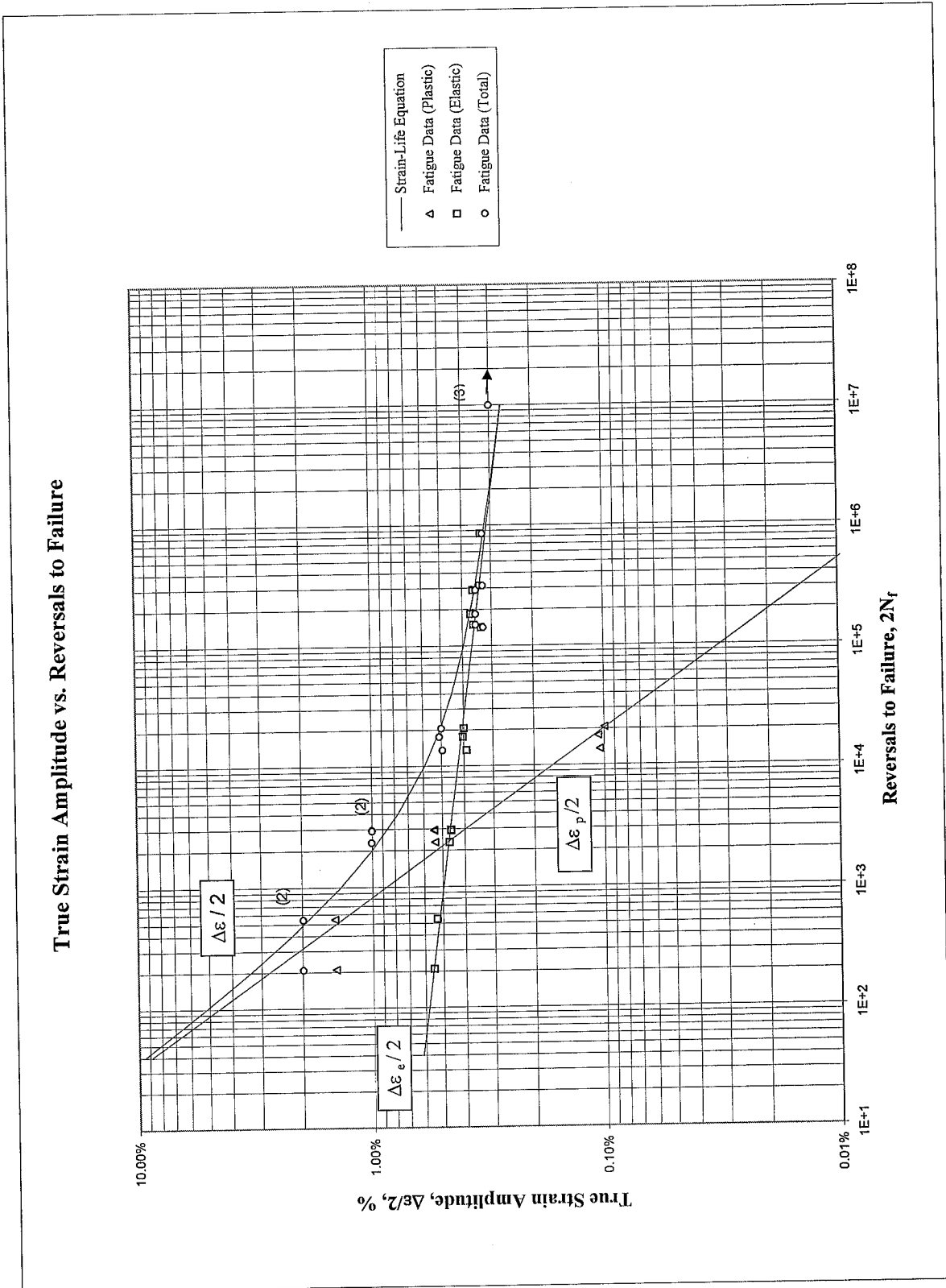


Figure 11: True strain amplitude versus reversals to failure

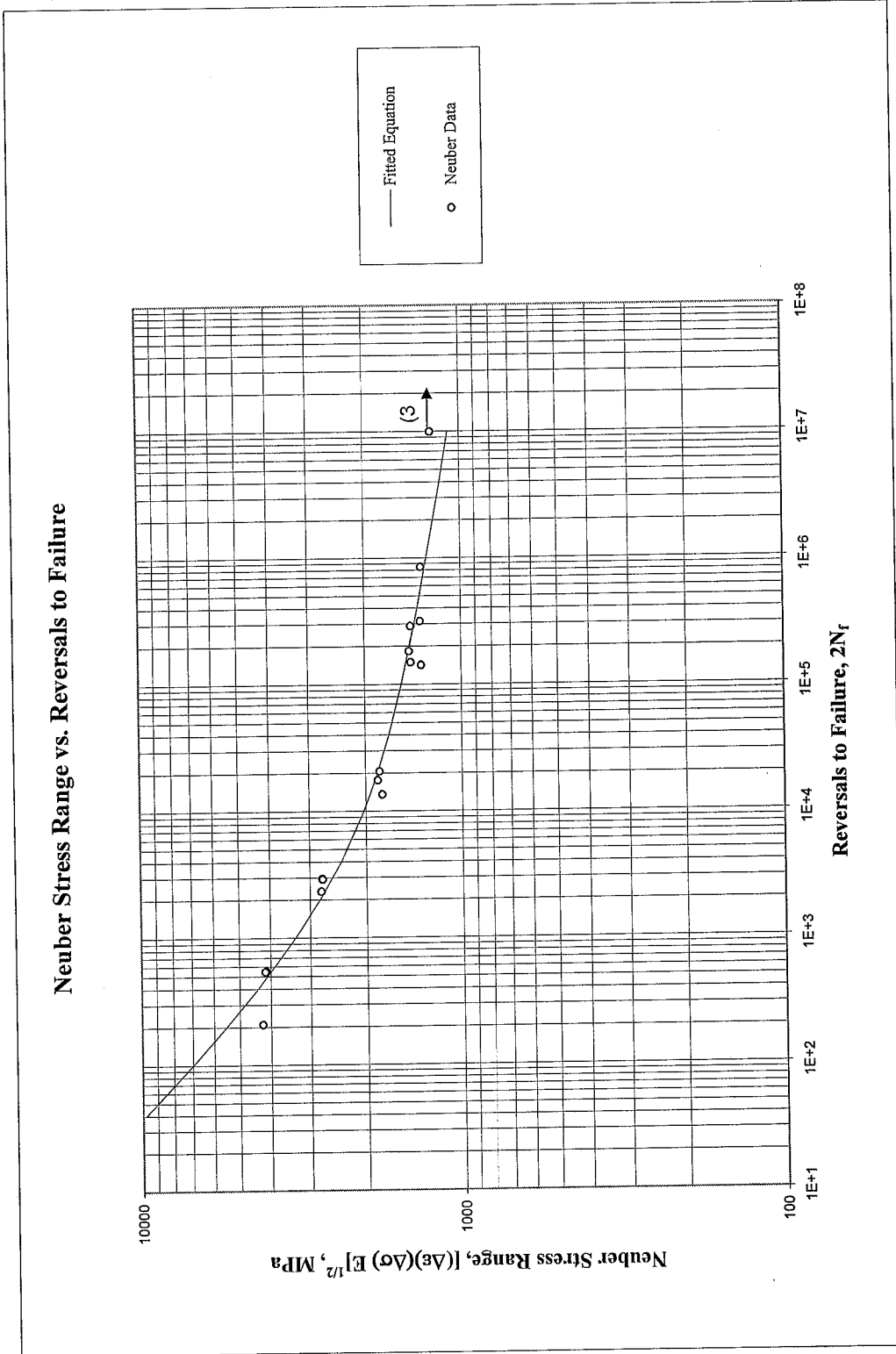


Figure 12: Neuber stress range versus reversals to failure



True Strain Amplitude vs. Reversals to Failure

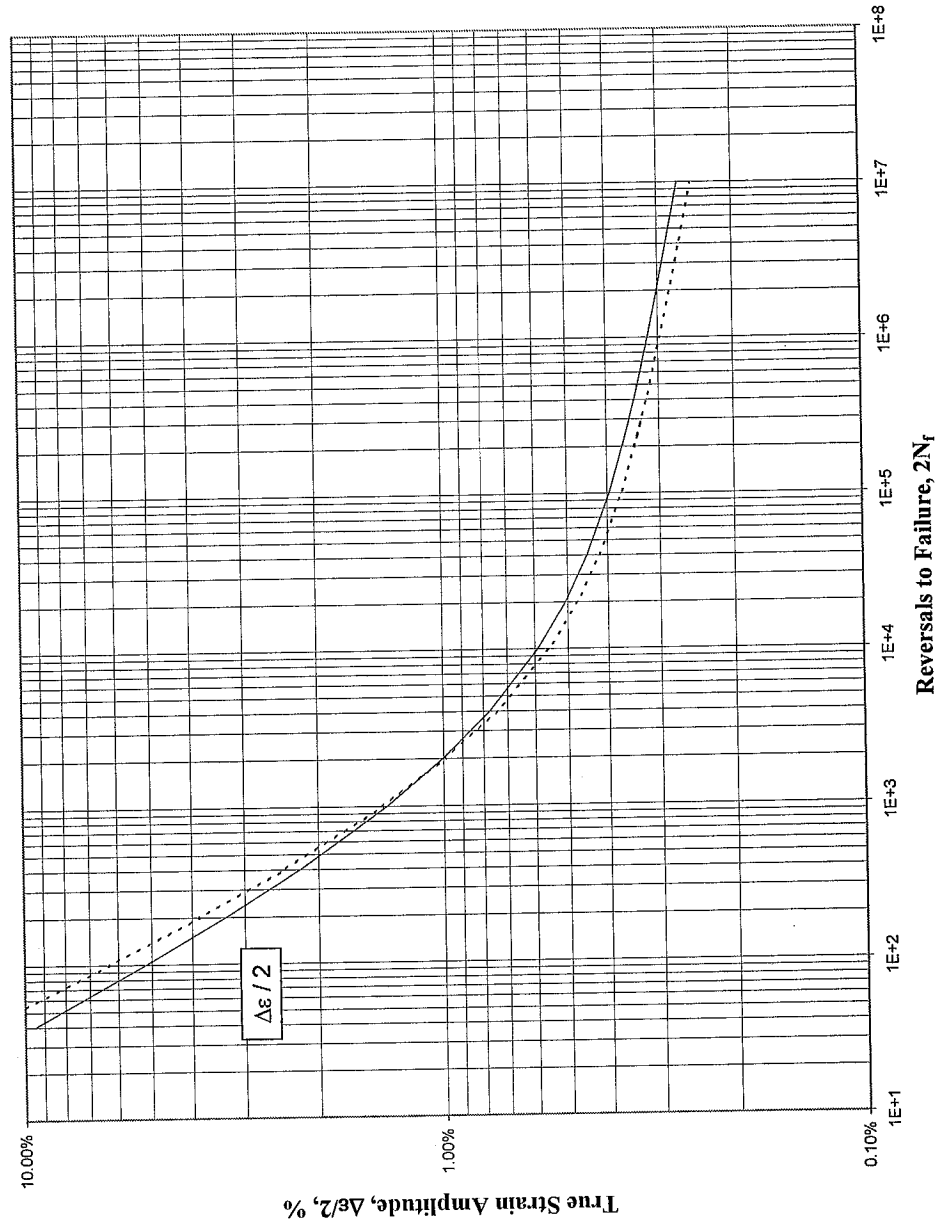


Figure 13: True strain amplitude versus reversals to failure

## REFERENCES

- [1] ASTM Standard E606-92, "Standard Practice for Strain-Controlled Fatigue Testing," Annual Book of ASTM Standards, Vol. 03.01, 1997, pp. 523-537.
- [2] ASTM Standard E83-96, "Standard Practice for Verification and Classification of Extensometers," Annual Book of ASTM Standards, Vol. 03.01, 1997, pp. 198-206.
- [3] ASTM Standard E1012-93a, "Standard Practice for Verification of Specimen Alignment Under Tensile Loading," Annual Book of ASTM Standards, Vol. 03.01, 1997, pp. 699-706.
- [4] ASTM Standard E8-96a, "Standard Test Methods for Tension Testing of Metallic Materials," Annual Book of ASTM Standards, Vol. 03.01, 1997, pp. 56-76.
- [5] ASTM Standard E112-96, "Standard Test Methods for Determining Average Grain Size," Annual Book of ASTM Standards, Vol. 03.01, 1997, pp. 227-249.
- [6] ASTM Standard E45-97, "Standard Test Methods for Determining the Inclusion Content of Steel," Annual Book of ASTM Standards, Vol. 03.01, 1997, pp. 157-170.
- [7] ASTM Standard E739-91, "Standard Practice for Statistical Analysis of Linear or Linearized Stress-Life (S-N) and Strain-Life ( $\epsilon$ -N) Fatigue Data," Annual Book of ASTM Standards, Vol. 03.01, 1995, pp. 615-621.
- [8] ASTM Standard E646-93, "Standard Test Method for Tensile Strain-Hardening Exponents (n-values) of Metallic Sheet Materials," Annual Book of ASTM Standards, Vol. 03.01, 1997, pp. 550-556.
- [9] Bridgman P. W., "Stress Distribution at the Neck of Tension Specimen," *Transactions of American Society for Metals*, Vol. 32, 1944, pp. 553-572.
- [10] Stephens R. I., Fatemi A., Stephens R. R. and Fuchs H. O., "*Metal Fatigue in Engineering*", Second edition, Wiley Interscience, 2000.

# APPENDIX

**Table A.1: Summary of monotonic tensile test results**

Specimen ID	D <sub>0</sub> , mm (in.)	D <sub>g</sub> , mm (in.)	L <sub>0</sub> , mm (in.)	L <sub>f</sub> , mm (in.)	E, GPa (ksi)	YS (offset=0.2%), MPa (ksi)	UYS, MPa (ksi)	LYS, MPa (ksi)	YPE, %	S <sub>u</sub> , MPa (ksi)	K, MPa (ksi)	n	%EL, %	%RA, %	R, mm (in.)	σ <sub>f</sub> *, MPa (ksi)	ε <sub>f</sub>
G4-23	5.245 (0.2065)	3.739 (0.1472)	7.620 (0.300)	9.525 (0.375)	201.2 (29,186.8)	1150.0 (166.8)	NA	NA	NA	1,243.3 (180.3)	1,498.3 (217.3)	0.0450	25.00%	49.19%	2.88 (0.113)	1311.3 (190.2)	67.70%
G4-19	5.093 (0.201)	3.747 (0.148)	7.620 (0.300)	9.449 (0.372)	203.7 (29,550.4)	1165.1 (169.0)	NA	NA	NA	1,252.4 (181.6)	1,498.6 (217.3)	0.0429	24.00%	45.88%	2.63 (0.104)	1311.3 (190.2)	61.40%
<b>Average values</b>					202.5 (29,368.6)	1157.5 (167.9)				1247.8 (181.0)	1498.5 (217.3)	0.0440	24.50%	47.53%	2.76 (0.109)	1311.3 (190.2)	64.55%

\* The values of true fracture strength are corrected for necking according to the Bridgman correction factor.

**Table A.2: Summary of constant amplitude completely reversed fatigue test results**

Specimen ID	Test control mode	Test freq., Hz	E, GPa (ksi)	At midlife ( $N_{50\%}$ )						$2N_{50\%}$ , [a]	$(2N_f)_{10\%}$ , [b]	$(2N_f)_{50\%}$ , [c]	Failure location [d]
				E', GPa (ksi)	$\Delta\epsilon/2$ , %	$\Delta\epsilon_p/2$ (calculated), %	$\Delta\epsilon_p/2$ (measured), %	$\Delta\sigma/2$ , MPa (ksi)	$\sigma_m$ , MPa (ksi)				
G4-4	strain	0.2	211.6 (30,690.0)	185.7 (26,928.5)	1.985%	1.462%	1.417%	1059.7 (153.7)	-15.6 (-2.3)	308	536	554	IGL
G4-8	strain	0.2	208.7 (30,270.0)	189.7 (27,511.5)	1.987%	1.438%	1.398%	1112.4 (161.3)	-18.5 (-2.7)	128	202	210	IGL
G4-9	strain	0.2	205.0 (29,730.0)	183.2 (26,563.5)	1.983%	1.454%	1.397%	1071.4 (155.4)	-21.2 (-3.1)	256	538	546	IGL
G4-11	strain	0.5	209.0 (30,310.0)	191.4 (27,760.0)	1.003%	0.538%	0.507%	941.5 (136.6)	-11.0 (-1.6)	1,024	2,268	2,338	IGL
G4-1	strain	0.5	205.4 (29,790.0)	187.6 (27,206.5)	1.001%	0.542%	0.505%	1071.4 (134.7)	-10.5 (-1.5)	1,200	2,824	2,952	IGL
G4-16	strain	0.5	202.9 (29,420.0)	189.1 (27,429.5)	0.999%	0.542%	0.493%	925.2 (134.2)	-10.3 (-1.5)	1,024	2,766	2,916	IGL
G4-17	strain	1	211.3 (30,650.0)	201.9 (29,282.5)	0.508%	0.106%	0.100%	814.8 (118.2)	8.7 (1.3)	8,192	16,938	17,664	IGL
G4-2	strain	1	210.1 (30,470.0)	199.2 (28,886.5)	0.493%	0.104%	0.096%	786.9 (114.1)	93.7 (13.6)	8,192	13,224	13,592	IGL
G4-10	strain	1	210.8 (30,580.0)	201.5 (29,217.0)	0.498%	0.099%	0.099%	807.0 (117.0)	-12.8 (-1.9)	10,604	20,436	20,708	IGL
G4-13	strain load	1.8 8	210.8 (30,570.0)	212.4 (30,802.0)	0.350%	0.000%	0.000%	741.8 (107.6)	57.5 (8.3)	1,508		183,468	IGL
G4-14	strain load	1.8 8	206.6 (29,960.0)	208.4 (30,231.0)	0.349%	0.000%	0.000%	725.5 (105.2)	58.6 (8.5)	1,246		289,798	IGL
G4-20	load	8			0.350%			724.0 (105.0)	0.0 (0.0)			149,734	IGL
G4-24	strain load	2.0 8	206.3 (29,920.0)	206.3 (29,917.5)	0.325%	0.000%	0.000%	669.7 (97.1)	18.7 (2.7)	2,232		850,728	IGL
G4-21	load	8			0.325%			672.3 (97.5)	0.0 (0.0)			142,640	IGL
G4-26	strain load	2.0 5	208.8 (30,280.0)	208.8 (30,277.5)	0.325%	0.000%	0.000%	678.6 (98.4)	6.6 (1.0)	1,362		315,010	IGL
G4-7	load	18			0.300%			620.6 (90.0)	0.0 (0.0)			>10,000,000	No Failure
G4-5	strain load	2.0 18	206.4 (29,940.0)	208.0 (30,168.0)	0.300%	0.000%	0.000%	620.8 (90.0)	42.7 (6.2)	1,134		>10,000,000	No Failure
G4-12	load	18			0.300%			620.6 (90.0)	0.0 (0.0)			>10,000,000	No Failure

[a]  $N_{50\%}$  is defined as the midlife cycle (for run-out tests, data is taken from the stable cycle indicated).

[b]  $(N_f)_{10\%}$  is defined as 10% load drop.

[c]  $(N_f)_{50\%}$  is defined as 50% load drop.

[d] IGL = inside gage length.

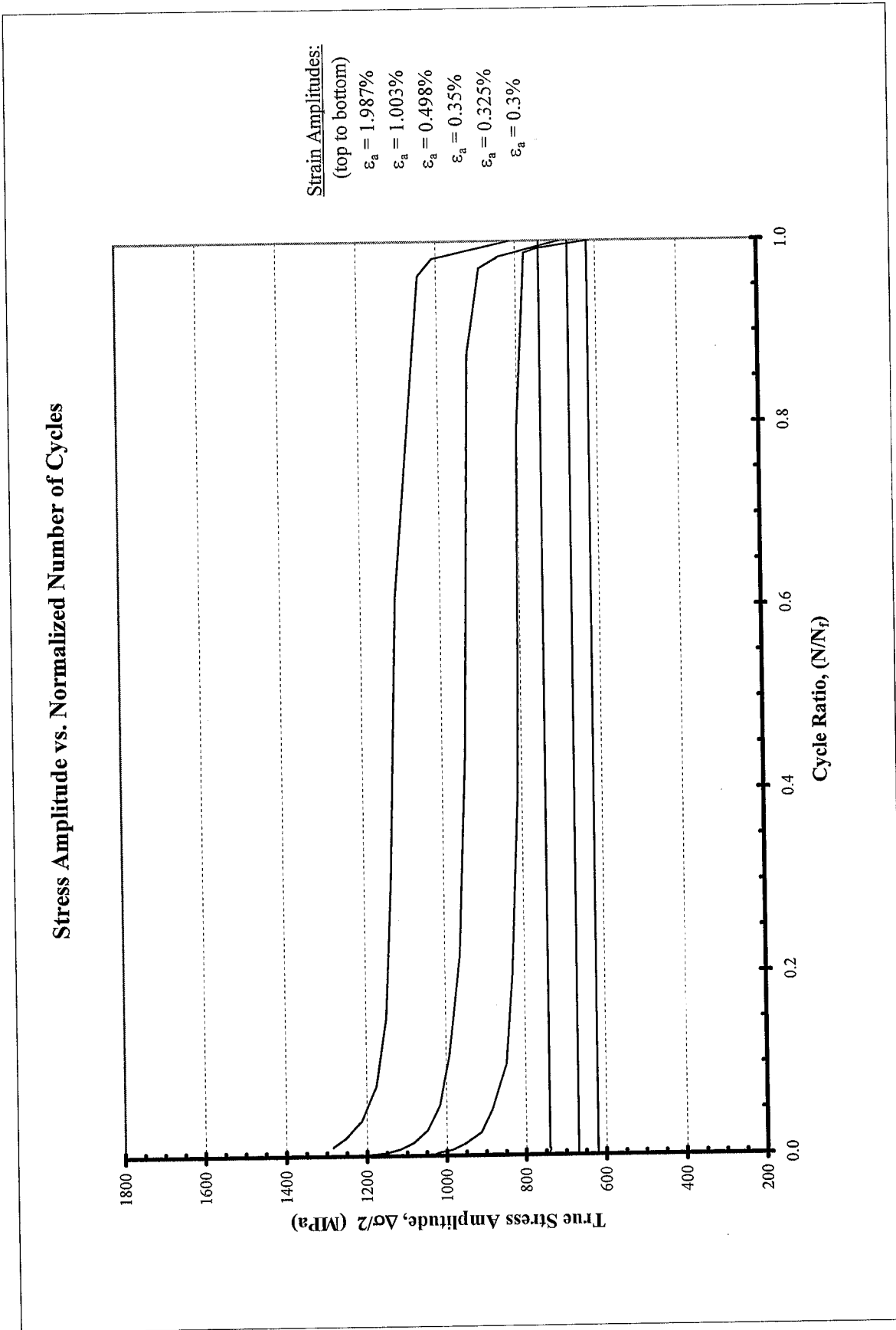


Figure A.1a: True stress amplitude versus normalized number of cycles

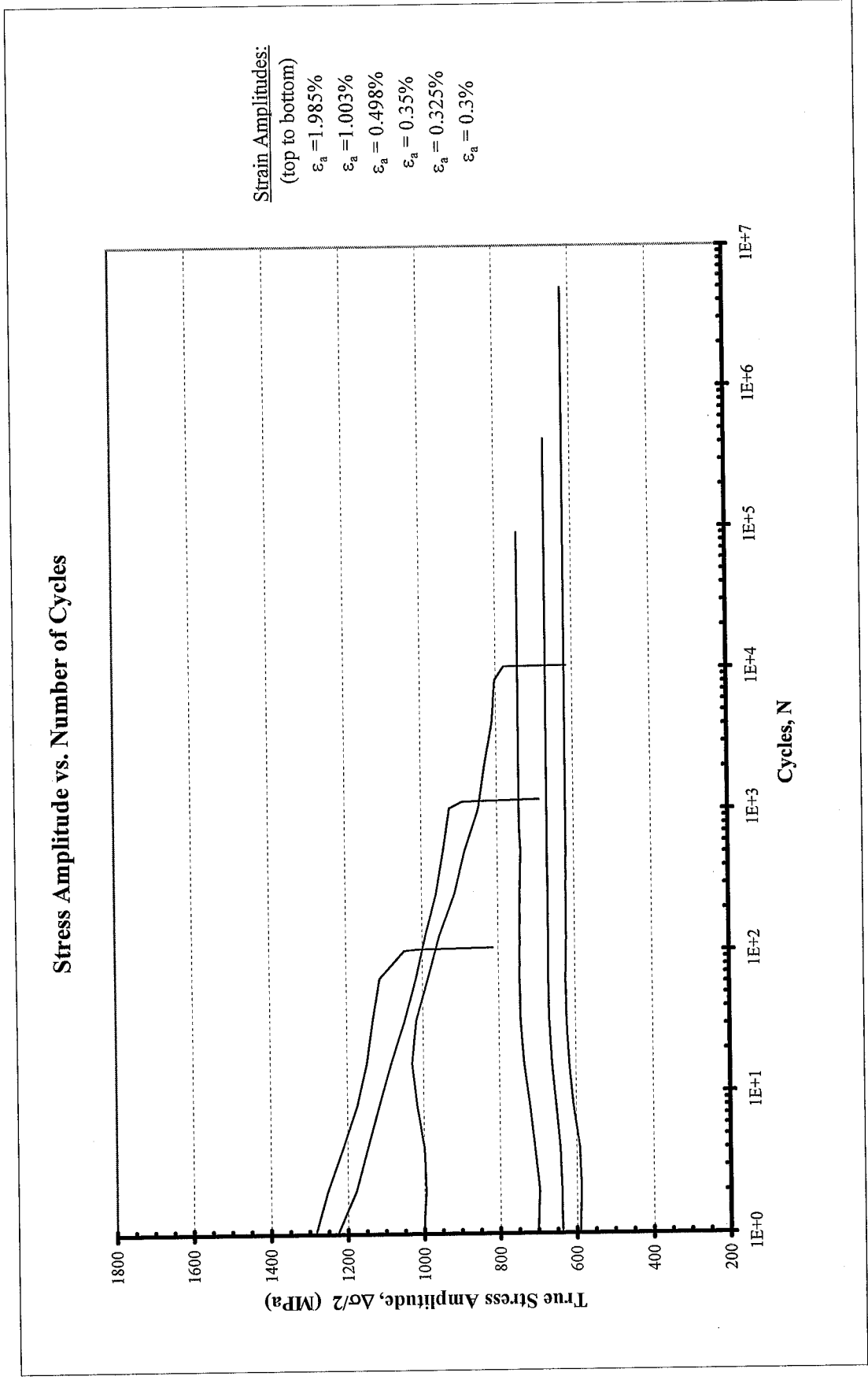


Figure A.1b: True stress amplitude versus number of cycles